AGU PUBLICATIONS

JGR

Journal of Geophysical Research: Space Physics

RESEARCH ARTICLE
10.1002/2017JA024194

Key Points:
- Latitudinal effect is important for the heliospheric current sheet (HCS) propagation
- Latitudinal effect is significant when a HCS has a small inclination angle
- The HCS inclination angle is better determined using the observation at 1 AU

Correspondence to:
Y. C.-M. Liu,
liuyong@spaceweather.ac.cn

Citation:
Peng, J., Liu, Y. C.-M., Huang, J., Li, H., Klecker, B., Galvin, A. B., … Zhang, J. (2017). In situ analysis of heliospheric current sheet propagation. *Journal of Geophysical Research: Space Physics*, *122*. https://doi.org/10.1002/2017JA024194

Received 28 MAR 2017
Accepted 11 SEP 2017
Accepted article online 4 SEP 2017

In Situ Analysis of Heliospheric Current Sheet Propagation

Jun Peng[1,2], Yong C.-M. Liu[1], Jia Huang[1,2], Hui Li[1], Berndt Klecker[3], Antoinette B. Galvin[4], Kristin Simunac[5], Charles Farrugia[4], L. K. Jian[6,7], Yang Liu[8], and Jie Zhang[9]

[1]State Key Laboratory of Space Weather, National Space Science Center, Chinese Academy of Sciences, Beijing, China, [2]College of Earth Science, University of Chinese Academy of Sciences, Beijing, China, [3]Max-Planck-Institut für Extraterrestrische Physik, Garching, Germany, [4]Institute for the Study of Earth Oceans and Space, University of New Hampshire, Durham, NH, USA, [5]Department of Natural Science, St. Petersburg College, Tarpon Springs, FL, USA, [6]Department of Astronomy, University of Maryland, College Park, MD, USA, [7]Heliophysics Science Division, NASA Goddard Space Flight Center, Greenbelt, MD, USA, [8]W. W. Hansen Experimental Physics Laboratory, Stanford University, Stanford, CA, USA, [9]Department of Physics and Astronomy, George Mason University, Fairfax, VA, USA

Abstract The heliospheric current sheet (HCS) is an important structure not only for understanding the physics of interplanetary space but also for space weather prediction. We investigate the differences of the HCS arrival time between three spacecraft separated in heliolongitude, heliolatitude and radial distance from the Sun (STEREO A, STEREO B, and ACE) to understand the key factors controlling the HCS propagation. By assuming that the source of the solar wind does not evolve except for the effects of solar rotation, we first test the first-order approach method (ignoring latitudinal differences), using STEREO observation during the year 2007, when the Sun was quiet and the two STEREO spacecraft were separated in heliolongitude by less than 44°. The first-order approach method matches well with observations for many events except for those events when the HCS has a small inclination angle to the ecliptic plane. The latitudinal effect is suggested to account for such discrepancies. The predictions are not improved much by considering the HCS inclination angle obtained from the potential field source surface (PFSS) model. However, the predictions match well with the observations when the HCS inclination angle at 1 AU is obtained from the time differences of HCS arrival times between the STEREO B and ACE spacecraft. An improved model of calculating the inclination of the heliospheric current sheet other than PFSS is needed.

1. Introduction

The heliospheric current sheet (HCS) is the boundary between oppositely directed heliospheric magnetic field lines (Smith, 2001). It is a continuous but wavy surface surrounding the Sun, which divides interplanetary space into two to four opposite polarity sectors in the ecliptic plane (e.g., Hundhausen, 1977; Levy, 1976; Owens & Forsyth, 2013; Schulz, 1973; Smith et al., 1978; Svalgaard & Wilcox, 1975; Thomas & Smith, 1981). Usually, the HCS is determined as the region where the heliospheric magnetic fields change sign and maintain the new polarity (Li, 2008).

The HCSs are significant for space weather predications. It is well known that geomagnetic storms are usually caused by reconnection of southward interplanetary magnetic fields with the magnetospheric field (Gonzalez et al., 1994; Tsurutani & Gonzalez, 1997). It is also documented that magnetic substorms are sometimes triggered by a northward turning of interplanetary magnetic field (McPherron et al., 1986). The HCS sometimes also lead to a sudden change of the magnetic field polarity. It is well known that polarity changes of the interplanetary magnetic field (IMF) may potentially cause a severe space weather event. HCSs interacting with CME-driven shocks may also lead to hazardous space weather events (Hu & Jia, 2001; Maynard et al., 2011).

The interaction of the HCS with cosmic rays has been well documented (Malova et al., 2016). A long-term correlation between the tilt of HCS and the cosmic ray intensity variations has been reported (Lockwood & Webber, 2005). Thomas et al. (2015) showed that the galactic cosmic ray intensity is modulated by HCSs over both decadal and short timescales. A recent study showed that lightning strikes are also modulated by HCSs (Owens et al., 2015). It is believed that HCSs may also be related with fundamental physics such as magnetic reconnection (Foullon et al., 2011; Gosling et al., 2005; Zharkova & Khabarova, 2012).

The stream interface (SI) is the boundary between the slow and fast solar wind (Burlaga, 1974; Gosling et al., 1978). Sometimes, the HCSs are found within a few hours from the SI, and they may even coincide with each

other as recent studies showed (Huang, Liu, & Klecker et al., 2016; Huang, Liu, & Qi et al., 2016). The evolution of stream interfaces was studied by Simunac et al. (2009) who concluded that in addition to radial and longitudinal separation between two spacecraft, the latitudinal separation and source evolution are also important for determining the propagation time between two spacecraft. We use HCS arrival times as an additional tool to study the latitudinal effects for the propagation of the solar wind in interplanetary space.

In this paper, we study HCS arrival time differences between different spacecraft to understand the solar wind propagation. The propagation time between these spacecraft is first predicted by assuming that both spacecraft are in the ecliptic plane and the source of the solar wind is stable. With these assumptions the time lapse is only determined by the radial and longitudinal separation. Second, the latitudinal differences of the spacecraft are taken into account. We show out that the latitudinal effect is significant when the HCS tilt angle is small. However, the HCS inclination angle predicted by the potential field source surface (PFSS) model (Schatten et al., 1969) may not reflect the inclination angle at 1 AU well. We tried to avoid magnetic flux that may distort the global magnetic field configuration. Simunac et al. (2009) concluded that some predicted propagation times do not match well with the observations because the solar wind source evolves. We draw a different conclusion in this study after we determine the inclination angle in a different way.

We also investigate a possible effect of the HCS type on the propagation time differences. HCS types are based on the relative locations of the HCS and true sector boundaries (TSBs). The TSB is defined as the boundary between sunward and antisunward flowing suprathermal electrons (Liu et al., 2014; Owens et al., 2013). Most of the suprathermal electrons are believed to flow out of the Sun's surface along the magnetic field lines, and therefore, the sector boundary should generally match well with the HCS. The cases where they mismatch are believed to be caused by rolling back magnetic field lines (Crooker et al., 2003), although Khabarova (2013) suggested that the mismatch was due to magnetic reconnection near 1 AU. If the nonideal HCSs can be explained by reconnection, then the predicted propagation time may not match well the observations since reconnection modifies the magnetic field configuration. We test the reconnection theory and the rolling back model with the HCS propagation time as well.

The data and instruments are presented in section 2. HCSs observations at each spacecraft are shown in section 3. The predicted propagation times and their comparison with observations are discussed in section 4. Conclusions are drawn in section 5.

2. Data and Instruments

The Solar Terrestrial Relations Observatory (STEREO) was launched in October 2006 and consists of two spacecraft. Both spacecraft orbit around the Sun with STEREO A (STA) leading ahead and STEREO B (STB) trailing behind the Earth. The longitudinal separation between STA and STB increases approximately at a rate of 45° per year (Kaiser et al., 2008). The Advanced Composition Explorer (ACE) is orbiting around the Lagrangian point L1 (Stone et al., 1998).

The data we used in this study are obtained during 2007. There are two reasons to choose the time period from March to December in 2007. First, the three spacecraft, STA, STB, and ACE, were still relatively close to each other, with a maximum separation in heliolongitude between STA and STB of 44°, and between STB and ACE of 23°. The assumption that the solar wind source does not evolve will more likely hold for a rather short propagation time difference corresponding to a small spacecraft separation. Second, the year of 2007 was during an extended solar minimum when very few coronal mass ejections (CMEs) were observed; therefore, it is an ideal time period to study the undisturbed solar wind. (Kilpua et al., 2009).

The data we use in this study are obtained from several instruments on board STEREO, including the In-situ Measurements of Particles and CME Transients (IMPACT) (Luhmann et al., 2008) and the Plasma and Suprathermal Ion Composition (PLASTIC) sensor (Galvin et al., 2008). The IMPACT instrument suite consists of six instruments to measure magnetic field and energetic particles. The suprathermal electron pitch angle distributions are obtained from the Solar Wind Electron Analyzer (SWEA) (Fedorov, 2011; Sauvaud et al., 2008) and the magnetic field is provided by the magnetometer (MAG) (Acuña et al., 2008). The kinetic properties of the solar wind used in this study are calculated from 1-D Maxwellian fits to the proton velocity distribution functions provided by PLASTIC (Simunac et al., 2009). Both the electron and proton data and magnetic field data have 1 min time resolution.

The ACE data were obtained from two instruments. The Solar Wind Electron, Proton, and Alpha Monitor (SWEPAM) (McComas et al., 1998) measures the in situ solar wind plasma and suprathermal electrons and the Magnetic Field Experiment (MAG) (Smith et al., 1998) detects the magnetic field. The plasma data have a 64 s time resolution, and the magnetic field data are obtained from 16 s averages.

In this study, we use the source surface magnetic field derived from the Wilcox Solar Observatory (WSO) synoptic charts which are obtained from http://wso.stanford.edu/synsourcel.html. The source surface field is computed from the WSO synoptic charts of photospheric magnetic field using a potential field source surface (PFSS) model (e.g., Altschuler & Newkirk, 1969; Hoeksema et al., 1983; Schatten et al., 1969). The PFSS model assumes that the magnetic field is potential between the photosphere and a spherical source surface. The modeled field matches the observed radial (or line-of-sight) magnetic field component on the photosphere and is forced to be purely radial at the source surface. It has been demonstrated that the locations of coronal holes, and the polarity and magnitude of the IMF, are well reproduced with the PFSS model with a source surface (Rss) set at 2.5 solar radii (e.g., Hoeksema, 1984; Lowder et al., 2014; Schrijver & De Rosa, 2003; Wang & Sheeley, 1992).

3. Observations

We identify HCSs based on four criteria to avoid local current sheets. First, the magnetic field changes sign and maintains the new polarity; second, the true sector boundary is in the vicinity; third, all three spacecraft observed the HCS consistently; and the fourth is the consistency with the WSO source surface. The first criterion is a general definition of the HCS. However, sometimes the HCS may have multilayered structures (Foullon et al., 2009), so using simply the polarity change alone may not be sufficient. The check of the consistency of the data from three spacecraft will also help us to exclude some local current sheets and make the comparisons possible. Since an HCS propagating with the solar wind usually arrives at the Earth in about 5 days, we look for the HCS which have corresponding neutral line crossing on WSO source surface field about 3–7 days (allowing for 2 days of uncertainty) ahead. These rules will help to exclude some local current sheets or transient structures.

Table 1 lists 35 HCSs we identified from March 2007 to December 2007. The HCS arrival time and the HCS type (introduced later in section 4.3) observed by STB, ACE, and STA are shown by the second, third, and fourth columns, respectively.

We also include some HCSs which do not have a corresponding crossing of the neutral line of the WSO source surface field, including events 17, 18, 21, 22, 25, and 26 in Table 1. These HCSs were observed by all three spacecraft and therefore were not likely to be local current sheets. On the other hand, although the track of the spacecraft does not appear to cross the neutral line in the synoptic map, the crossing might have occurred, considering the uncertainty of calculating the neutral line and the crossing point.

4. Methods

This part includes four sections. Two types of analysis will be done in the following sections; without considering the latitude of spacecraft in section 4.1, and with considering the latitude of spacecraft in section 4.2. In section 4.3, we discuss the effect of the HCS type. In section 4.4, we introduce a new method to predict time difference between two spacecraft.

4.1. First-Order Propagation Time

Under the assumptions that the Sun rotates rigidly, the solar wind sources do not evolve, and all spacecraft have the same latitudes, the first-order propagation time is determined by the radial and longitudinal separation between spacecraft. The total sums up the longitudinal time difference Δt_φ and radial time difference Δt_r. Their relationship, as shown in Figure 1, is as follows:

$$\Delta t = \Delta t_r + \Delta t_\varphi. \tag{1}$$

where

$$\Delta t_\varphi = \varphi/\omega_{\mathrm{Sun}} \tag{2}$$

Table 1
Summary List of Heliospheric Current Sheets During March 2007 to December 2007

	STEREO B		ACE		STEREO A	
No.	HCS arrival time (UT)	Type	HCS arrival time (UT)	Type	HCS arrival time (UT)	Type
1	2007/3/11; 19:00	NA	2007/3/11; 17:20	a	2007/3/11; 16:26	a
2	2007/3/22; 01:25	e	2007/3/21; 20:30	a	2007/3/21; 21:16	a
3	2007/3/25; 00:30	b	2007/3/24; 22:00	b	2007/3/24; 14:10	b
4	2007/4/1; 01:30	a	2007/3/31; 22:15	a	2007/3/31; 22:15	c
5	2007/4/9; 05:20	e	2007/4/9; 0:15	a	2007/4/8; 20:50	e
6	2007/4/17; 06:30	a	2007/4/17; 2:30	a	2007/4/17; 2:20	a
7	2007/4/22; 12:14	c	2007/4/22; 4:30	a	2007/4/21; 23:40	a
8	2007/4/26; 17:50	b	2007/4/26; 17:50	a	2007/4/26; 18:40	c
9	2007/5/7; 12:25	a	2007/5/7; 9:50	c	2007/5/7; 10:00	e
10	2007/5/14; 09:50	b	2007/5/14; 9:15	b	2007/5/14; 9:00	a
11	2007/5/18; 06:25	a	2007/5/18; 7:40	a	2007/5/18; 13:40	a
12	2007/5/23; 04:25	b	2007/5/23; 9:30	b	2007/5/23; 17:05	b
13	2007/6/2; 00:55	b	2007/6/1; 19:10	b	2007/6/2; 17:55	NA
14	2007/6/8; 03:55	a	2007/6/8; 0:25	a	2007/6/8; 5:05	a
15	2007/6/13; 14:40	a	2007/6/13; 18:00	a	2007/6/14; 1:05	a
16	2007/6/21; 03:30	a	2007/6/21; 6:40	e	2007/6/21; 18:15	a
17	2007/6/28; 16:15	a	2007/6/28; 22:10	c	2007/6/30; 3:40	a
18	2007/7/2; 20:05	b	2007/7/3; 10:00	a	2007/7/3; 16:20	a
19	2007/7/10; 20:15	a	2007/7/11; 0:10	a	2007/7/11; 10:35	a
20	2007/7/19; 01:30	e	2007/7/19; 2:40	b	2007/7/20; 12:35	a
21	2007/7/26; 08:25	a	2007/7/26; 15:20	a	2007/7/27; 4:50	a
22	2007/7/28; 18:05	a	2007/7/29; 0:15	a	2007/7/29; 8:25	a
23	2007/8/5; 12:20	b	2007/8/6; 2:55	e	2007/8/7; 4:20	e
24	2007/8/14; 17:25	a	2007/8/15; 0:45	a	2007/8/16; 4:59	a
25	2007/8/24; 05:00	a	2007/8/24; 11:50	a	2007/8/25; 11:55	a
26	2007/8/24; 14:55	a	2007/8/25; 11:25	a	2007/8/25; 23:25	a
27	2007/8/31; 16:10	b	2007/8/31; 19:45	c	2007/9/1; 14:25	c
28	2007/9/13; 10:15	e	2007/9/13; 22:00	e	2007/9/14; 16:50	b
29	2007/9/26; 18:05	a	2007/9/27; 14:00	c	2007/9/28; 17:45	a
30	2007/10/10; 06:15	e	2007/10/11; 8:40	e	2007/10/12; 20:55	b
31	2007/10/23; 16:45	c	2007/10/24; 20:10	c	2007/10/25; 18:15	e
32	2007/11/7; 18:00	a	2007/11/8; 9:20	b	2007/11/9; 10:50	c
33	2007/11/19; 15:50	a	2007/11/20; 11:55	a	2007/11/21; 3:15	a
34	2007/11/29; 15:04	c	2007/12/1; 8:30	c	2007/12/2; 17:35	b
35	2007/12/15; 23:20	a	2007/12/17; 4:53	a	2007/12/18; 12:35	a

and

$$\Delta t_r = \Delta s / v_B \tag{3}$$

Here φ is the separation in longitude of STA and STB in the Heliocentric Inertial (HCI) coordinate system. ω_{Sun} is the average angular velocity of 13.3° per day at 1 AU of the solar equator. Δs is the radial difference from the Sun between STA and STB defined as $r_A - r_B$. The radial distance Δs is always negative since STA is closer to the Sun. The longitudinal difference Δt_φ is usually positive since STA is the leading spacecraft. When Δt is positive (negative), STA observed the HCS later (earlier) than STB. v_B is the bulk speed of solar wind observed by STB. This method was also documented in Opitz et al. (2009).

Figure 2 shows the predicted and observed propagation times. During March and April of 2007, the propagation time Δt is negative for some events. When the two spacecraft were separated by more than 5.5°, Δt stays positive. The results show that the predicted time difference has the same trend as the observed time difference, but there are two periods in which the predicted time differences were far from the observed ones as marked by the pink regions. The first period corresponds to Events 27 and 28 in September 2007, and the second corresponds to Events 31, 32, and 33 in October and November 2007. Simunac et al. (2009) have analyzed the SI evolution, and they found that the predicted SI crossing time differences also deviated from the observations during the same time periods. They suggested that the deviations in the first period can be explained by latitudinal differences between the spacecraft, but the second period may be caused by other factors like the evolution of the source region. We will consider the latitudinal difference in the next section.

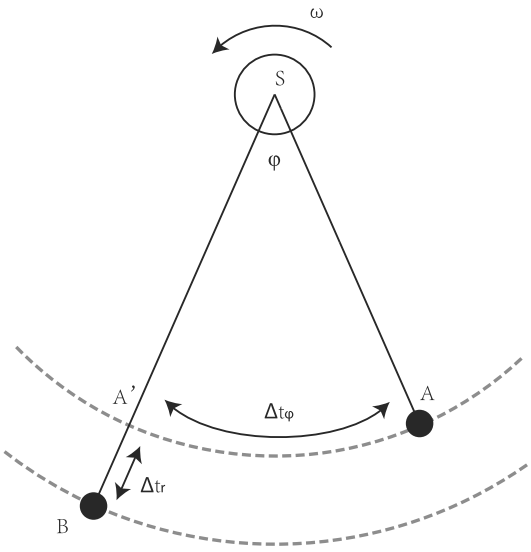

Figure 1. Sketch of two spacecraft (STA and STB) at the same HCI latitude, separated in radial distance and longitude φ. The schematic illustrates the time difference from the longitudinal spacecraft separation t_φ and the time difference from the radial spacecraft separation t_r, and ω refers to the solar rotation. Reproduced from Opitz et al. (2009).

4.2. Latitudinal Effects

The propagation time due to the latitudinal differences is denoted by Δt_θ, now the total difference is calculated as follows:

$$\Delta t^{'} = \Delta t_r + \Delta t_\varphi + \Delta t_\theta \tag{4}$$

As shown in equation (5) and Figure 3, the latitudinal difference of the spacecraft combined with an oblique HCS will result in an additional longitudinal separation $\Delta\varphi'$, which is calculated as

$$\Delta\varphi^{'} = \theta \times \cot \Psi \tag{5}$$

where Ψ is the inclination angle of the HCS. The corresponding propagation time due to the latitudinal difference is then

$$\Delta t_\theta = \frac{\theta \times \cot \Psi}{\omega_{\mathrm{Sun}}}. \tag{6}$$

Equation (6), consistent with the analysis in Simunac et al. (2009), shows that the latitudinal effect is significant when HCS inclination angle is small.

To obtain the inclination angle Ψ of the HCS, we obtain the inclination angle of the HCS from the WSO source surface magnetic field as a proxy of the inclination angle at 1 AU. The back mapping technique is used to obtain the intersection between the HCS and the spacecraft trajectory. It is a simple ballistic method that assumes the solar wind propagates with constant speed radially outward from the solar source surface (Nolte & Roelof, 1973).

When STA observes an HCS, STB would observe an HCS of the same sector close in time, in general. Figure 4 shows the WSO source surface magnetic field of the 35th case. In this case, STB has a higher latitude than STA. The upper blue horizontal line is the latitude of STB, it crosses with the neutral line in point B. The lower red horizontal line is the latitude of STA, it crosses the neutral line in point A. Combining point A and B, and we get line AB. Because point A and point B are close to each other, the inclination of line AB can be regarded as the inclination of the HCS; that is, the inclination of line AB is equal to Ψ (in this case it is an obtuse angle). In

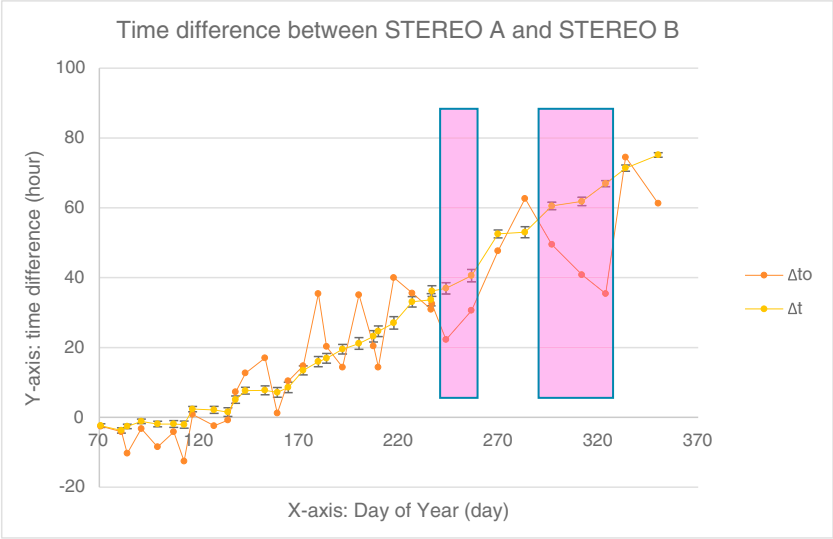

Figure 2. Observed and predicted propagation time difference between of STA and STB. *X* axis is the day of year 2007, and *y* axis is time difference. The orange line is the observed time difference Δt_o between two spacecraft; the yellow line is the time difference Δt using the first-order approach method, that is, neglecting latitudinal effects. In most cases observed and predicted times show a good agreement, with time differences of less than 1 day. However, there are two periods in which the predicted time differences were far from the observed ones as marked by the pink region.

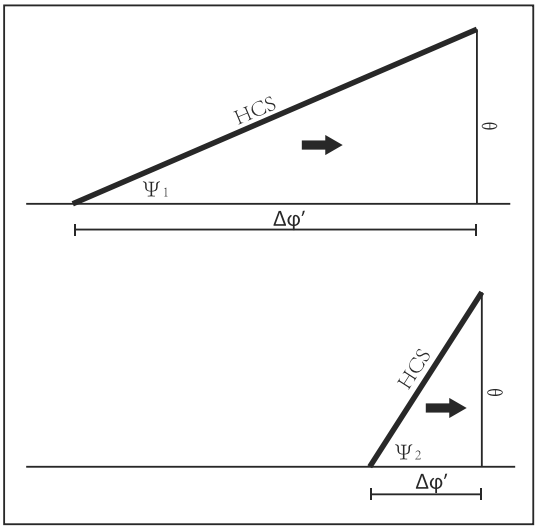

Figure 3. Schematic to demonstrate the time difference due to the slope of the HCS in the latitude-longitude plane. The HCS is the thick black oblique line, and Ψ is the oblique angle. The arrow pointing to the right indicates the direction of HCS propagation; θ is the latitudinal difference. This figure illustrates the additional longitudinal separation due to the latitudinal difference of two spacecraft and an oblique HCS. The line segment labeled Δt_φ shows the additional longitudinal separation as a function of θ and Ψ. In the top panel, the HCS has a smaller angle Ψ than in the bottom panel. The two panels show that for the same latitudinal difference, the smaller angle Ψ results in a larger additional longitudinal separation.

the WSO source surface field, we can calculate the Ψ angle by unifying the unit of horizontal and vertical axis. It is easy to obtain

$$\Delta t_\theta = T_{A(\mathrm{wso})} - T_{B(\mathrm{wso})}. \quad (7)$$

If the HCS has an acute angle or STB has a lower latitude than STA, we will come up with the same result.

We now compare observed and predicted HCS arrival times for STA and STB (Figure 5). The orange line is the observed time difference between two spacecraft; the yellow line is the time difference calculated with the classical method; the green line is the expected time difference with the method which includes the latitude effect. In most cases the two methods show good agreement with less than 1 day difference between predicted and observed times. For 9 events the agreement considering latitude effects is better, for 14 events the agreement is better, not considering latitude effects, and for the remaining 12 events there is no difference. No difference means that the difference caused by the latitude effect is zero. There are two reasons for this, the first is that the latitude separation of the two spacecraft is less than the pixel resolution of the WSO synoptic chart of 0.58° and the second is that their latitude is larger than the maximum peak of the neutral line or smaller than the minimum peak of the neutral line. The latitude relation of the three spacecraft is shown in Figure 6.

The same method can also be used for STB and ACE. The results are shown in Figure 7 using the same format as Figure 5. For 8 events the agreement considering latitude effects is better; for 15 events the agreement is better, not considering latitude effects; and for the remaining 12 events there is no difference.

In general, including latitudinal effects does not improve the propagation time prediction. In some cases, the prediction becomes even worse than the first-order approach.

4.3. HCS's Type Effect

There are five types of HCSs based on the relative locations of HCS and TSB as classified by Owens et al. (2013), called types (a) (b) (c) (d), and (e). These five types, are shown in Figure 8, reproduced from

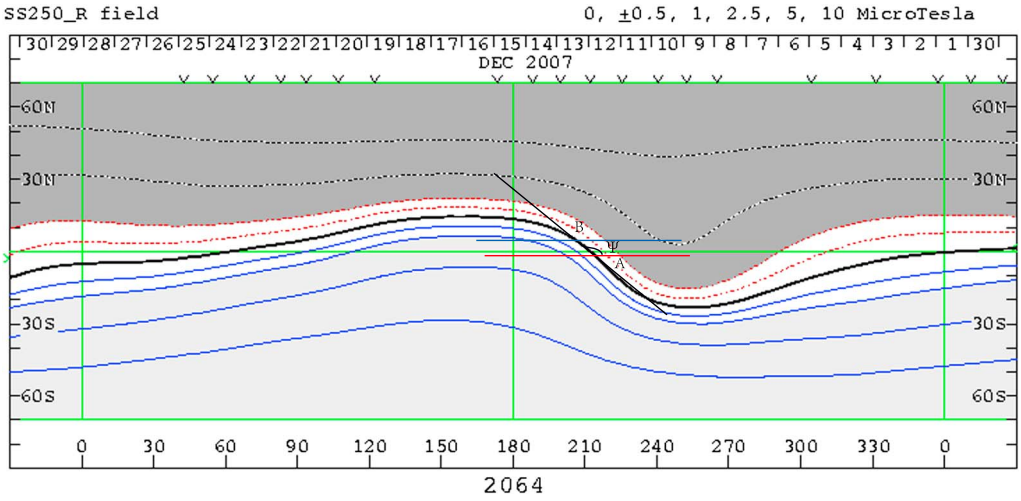

Figure 4. It shows the 35th case of Table 1 in the WSO synoptic chart of Carrington rotation 2064. In this case, STB has a higher latitude than STA. The upper blue horizontal line is the latitude of STB; it crosses the neutral line in point B. The lower red horizontal line is the latitude of STA; it crosses the neutral line in point A. Line AB has Ψ angle with the red horizontal line.

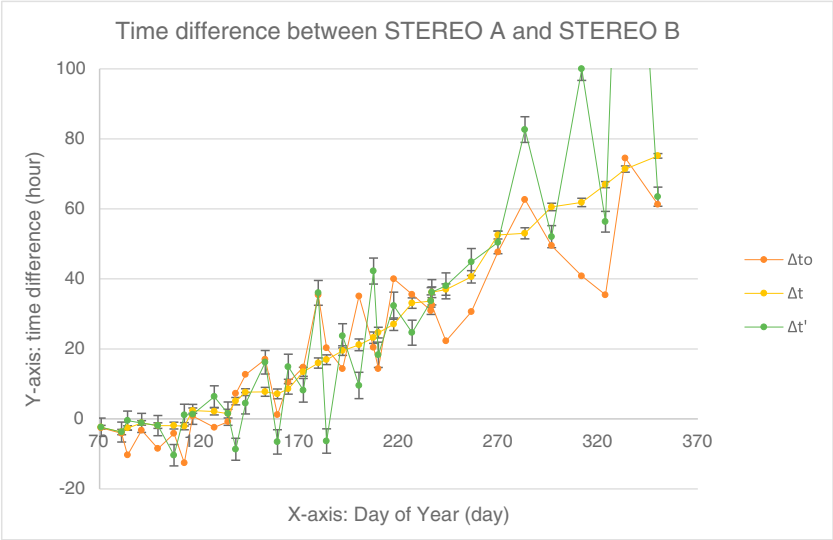

Figure 5. Observed and predicted propagation time difference between STA and STB. The orange line is the observed time difference Δt_o between two spacecraft; the yellow line is the calculated time Δt using the first-order approach method; the green line is the expected time difference $\Delta t'$ including the latitude effect.

Owens et al. (2013). In general, type (a) and type (c) HCS are considered as ideal HCSs implying that there are no rolling back magnetic field lines and HCS coincides with the TSB (Huang, Liu, & Qi et al., 2016; Liu et al., 2014; Owens et al., 2013). Types (b), (d), and (e) are nonideal, because the HCS is separated from the TSB or even no TSB is observed. To investigate whether the HCS types affect the propagation time, we plot predicted and observed propagation times separately for ideal HCS (Figure 9a) and for nonideal HCS (Figure 9b).

The comparison shows little difference for ideal and nonideal HCS events. For ideal events, there are also some cases when the predicted time was far off the observed time. For nonideal events, there are also cases when the prediction matches pretty well with the observations. It could be that the types of HCS were formed at a position near the Sun. If so, the HCS types would not modify the propagation time near 1 AU. Reconnection here may not be the cause for those events with separated HCS and TSB.

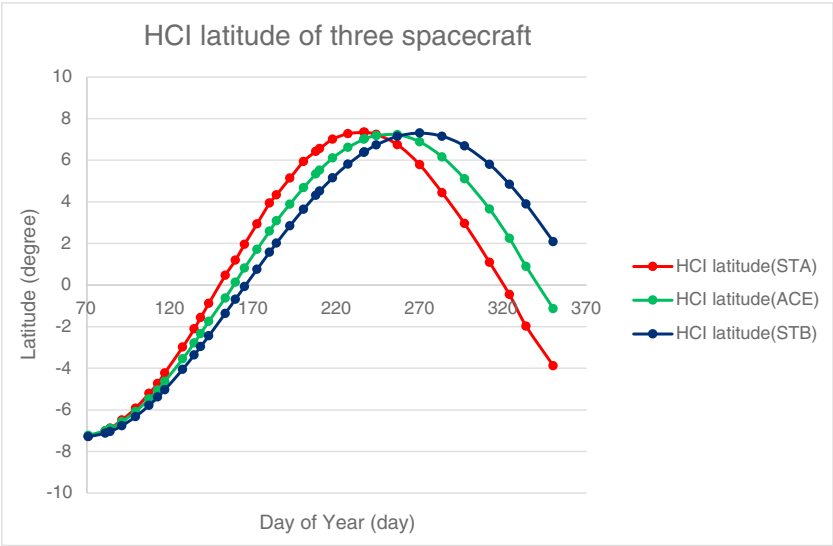

Figure 6. The latitude of STA, ACE, and STB in HCI coordinates in 2007.

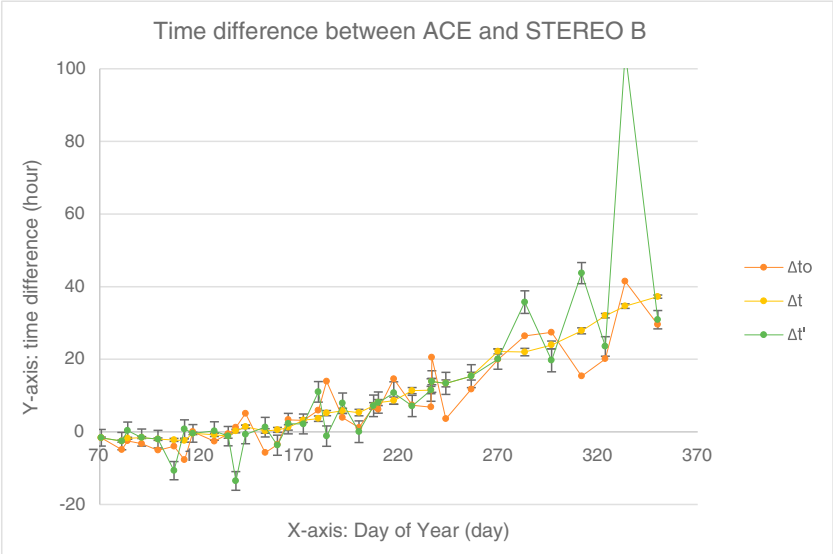

Figure 7. Same format as Figure 5 but for comparison between ACE and STB.

4.4. Discussion

When calculating the latitudinal effect in section 4.2, the HCS inclination angle Ψ is inferred using the WSO source surface field. However, the obtained angle may not reflect the actual HCS angle for the observed events at 1 AU. We now infer the HCS angle using the observations of STB and ACE. We assume that all differences between the observed and predicted propagation times using equation (1) are due to the latitudinal effects defined by equation (5).

The observed time difference from STB to ACE is noted as Δt_o(BC), and that predicted Δt(BC), the difference between them is $\Delta t_\theta'$(BC), so we have

$$\Delta t_\theta'(\mathrm{BC}) = \Delta t_o(\mathrm{BC}) - \Delta t(\mathrm{BC}) \tag{8}$$

With the assumption that all deviations are due to latitude differences, the inclination angle Ψ' of the HCS at 1 AU can be determined as

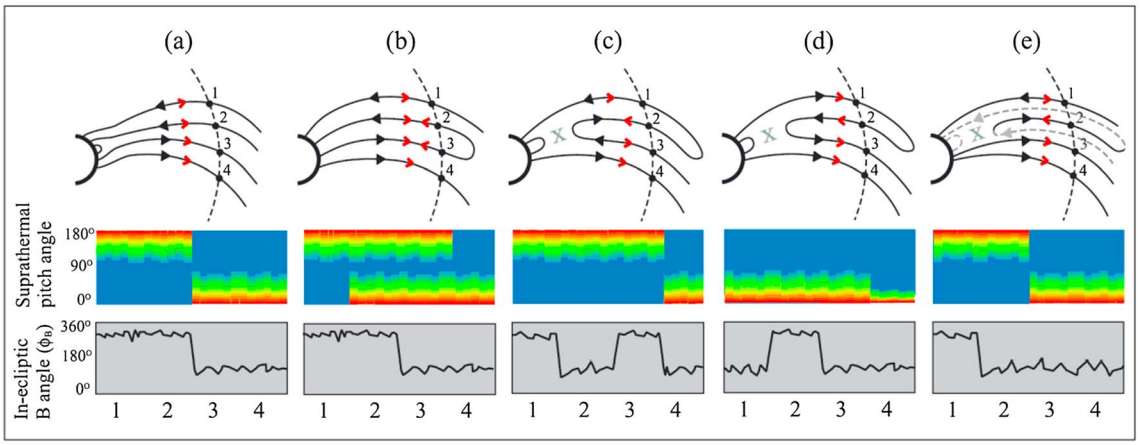

Figure 8. Sketches of five possible heliospheric magnetic field configurations and the resulting magnetic field and suprathermal electron signatures in near-Earth space. Red (black) arrows show the thermal electron strahl (magnetic field polarity), while gray crosses show the position of magnetic reconnection. Type (a): a typical sector boundary/HCS crossing. Type (b): a sector boundary accompanied by closed HMF loops, likely part of an interplanetary coronal mass ejection (ICME). Type (c): a sector boundary/HCS crossing containing an inverted HMF interval at time 2. Type (d): an inverted HMF interval at time 2 embedded within a unipolar region. Type (e): a sector boundary with mismatched electron and magnetic signatures. The dashed lines show portions of the inverted HMF structure which are out of the ecliptic plane and not encountered by the observing spacecraft. From Owens et al. (2013).

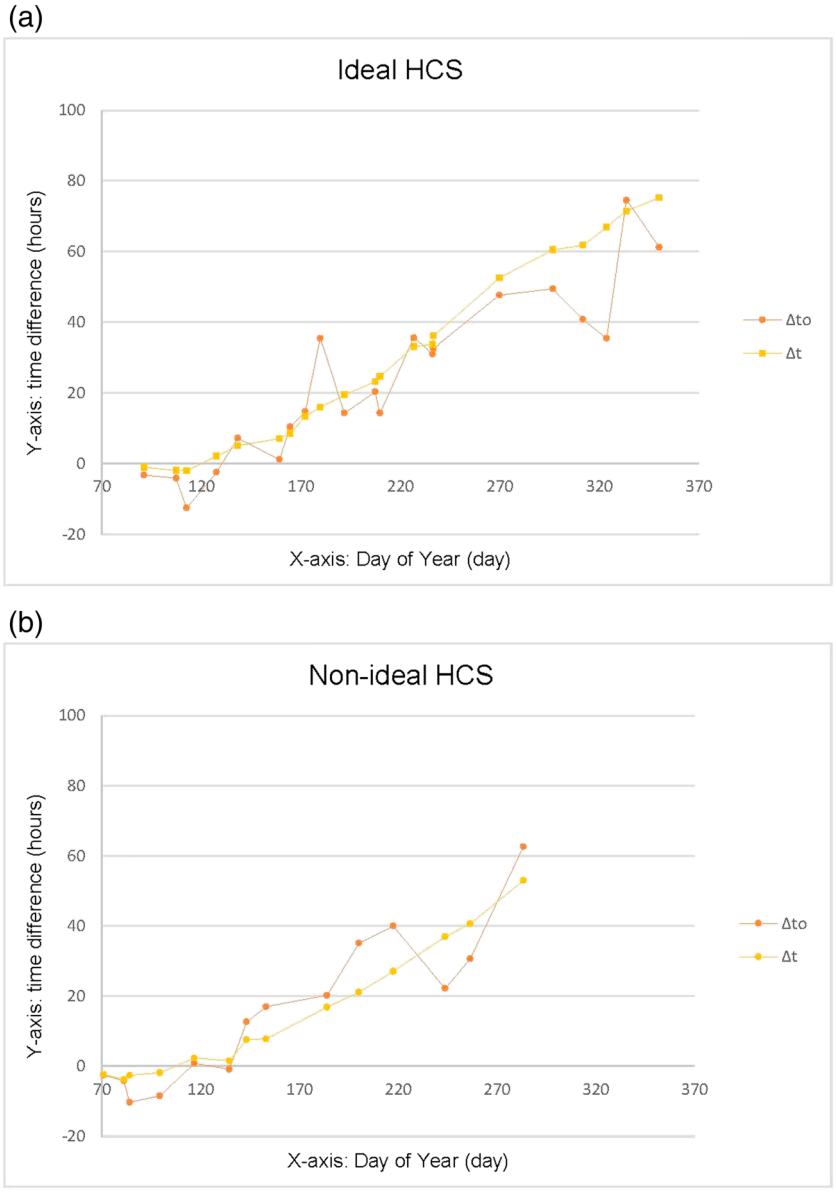

Figure 9. (a) Observed and predicted propagation time difference between STA and STB for ideal HCS. The orange line is the observed time difference Δt_o between two spacecraft; the yellow line is the expected time difference with the first-order approach method Δt. (b) Same format as Figure 9a but for nonideal HCS.

$$\cot \Psi' = \Delta t'_{\theta}(\mathrm{BC}) \times \frac{\omega_{\mathrm{Sun}}}{|\theta_{\mathrm{BC}}|}. \tag{9}$$

With the Ψ' angle of HCS, we get the latitude time difference between STB and STA,

$$\Delta t'_{\theta}(\mathrm{BA}) = \cot \Psi' \times \frac{|\theta_{\mathrm{BA}}|}{\omega_{\mathrm{Sun}}}, \tag{10}$$

The predicted propagation time is now

$$\Delta t''(\mathrm{BA}) = \Delta t_r(\mathrm{BA}) + \Delta t_{\varphi}(\mathrm{BA}) + \Delta t'_{\theta}(\mathrm{BA}). \tag{11}$$

The further improved predicted time differences $\Delta t''$ are plotted together with the observations in Figure 10. Obviously, the new predictions (blue line) match with the observations much better than the previous ones.

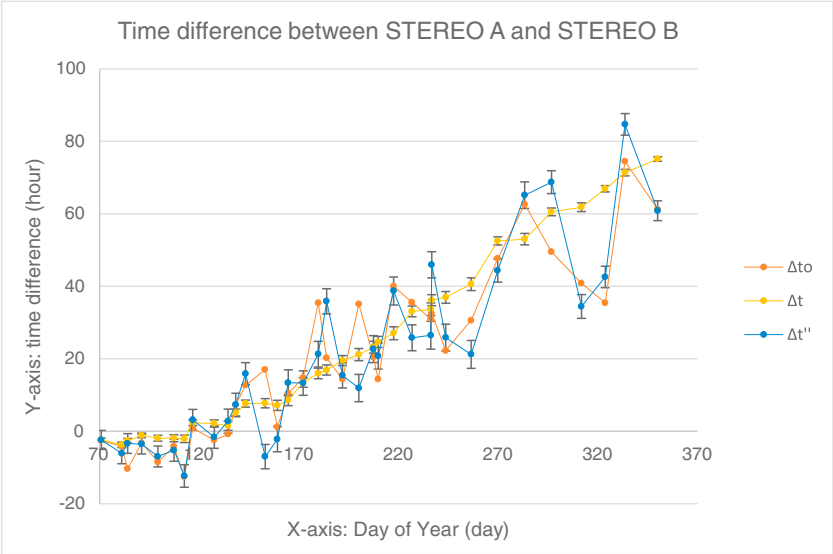

Figure 10. Observed and predicted propagation time difference between STA and STB with the new method. The orange line is the observed time Δt_o between the two spacecraft; the yellow line is the calculated time with the first-order approach method Δt; the blue line is the calculated time with the new method $\Delta t''$.

Note that in the events marked by the pink region in Figure 2, now prediction matches with the observations very well.

For 22 events the agreement is now better, and for 13 events the agreement is worse. For the time periods when the first-order method, and even the method including the latitudinal effects failed, the new predicted propagation times follow the observed trend very well, and we fixed the events with large discrepancy, although we may not be able to fix some smaller errors.

Figure 11 shows the inclination angles from WSO and from in situ observations. The two lines have only low correlation, for events 2, 4, 6, 14, 16, 20, 23, 24, 28, 31, and 32, the inclination angles even have an opposite sign.

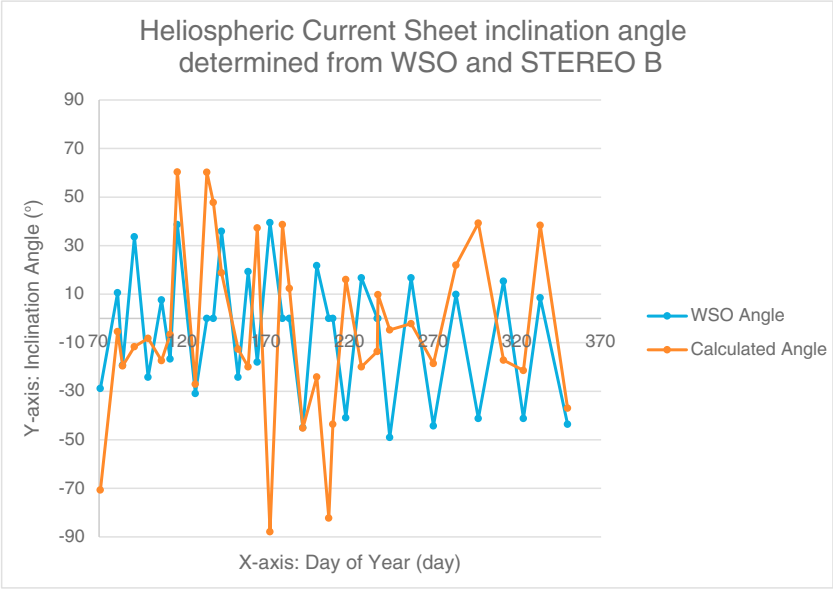

Figure 11. Comparison between the inclination angles obtained from WSO (blue line) versus inclination angles calculated from in situ observations (orange line). *X* axis is the day of year. *Y* axis is the inclination angle.

5. Summary and Conclusions

We investigate the arrival time difference for 35 HCSs between STA and STB during the year of 2007. To accurately predict the HCS propagation time, we start with a first-order approach which considers only radial and longitudinal differences. The first-order approach matches with the observations reasonably well, except for two major periods when the predicted values are significantly smaller than the observed time differences. The latitudinal effects are then considered, using two estimates for the HCS inclination angles Ψ: (1) Ψ is calculated using the WSO source surface field and (2) Ψ is inferred from the propagation time between STB and ACE, both spacecraft located at ~1 AU. The predictions match very well with the observations only when we use the inclination angles of the HCS as obtained from method (2). Therefore, we make the following conclusions:

1. The latitudinal effects are significant in determining the HCS propagation time, especially when the HCS inclination angle is small.
2. The HCS inclination angle determined by the WSO source surface field does not accurately reflect the situations at 1 AU for some events; the predictions using 1 AU observations are better. The WSO chart may not reflect the HCS inclination at 1 AU; how to determine the inclination angle requires further study.
3. The types of HCSs have little effects on their propagation times, and the mismatch of the HCSs is unlikely to be caused by reconnection in the vicinity of 1 AU.

Acknowledgments
This work is supported by the Chinese Academy of Science "Hundred Talented Program," the Chinese National Science Foundation of contracts 41674173 and 41574169, and the Specialized Research Fund for State Key Laboratory of China. This work is also supported by STEREO and Wind grants to UNH. This work is also supported by The Chinese National Science Foundation grant AGS 1259549 and NASA's Science Mission Directorate as part of the STEREO project. The in situ data are provided by the STEREO (http://stereo-ssc.nascom.nasa.gov), Wind (http://pwg.gsfc.nasa.gov/wind.shtml), and ACE (http://www.srl.caltech.edu/ACE/ASC/) Science Center. We also thank Stanford University for the WSO source surface field, and SolarSoft library for the PFSS model.

References

Acuña, M. H., Curtis, D., Scheifele, J. L., Russell, C. T., Schroeder, P., Szabo, A., & Luhmann, J. G. (2008). The STEREO/IMPACT magnetic field experiment. In C. T. Russell (Ed.), *The STEREO Mission* (pp. 203–226). New York: Springer. https://doi.org/10.1007/978-0-387-09649-0_8

Altschuler, M. D., & Newkirk, G. (1969). Magnetic fields and the structure of the solar corona. I: Methods of calculating coronal fields. *Solar Physics*, *9*(1), 131–149. https://doi.org/10.1007/BF00145734

Burlaga, L. F. (1974). Interplanetary stream interfaces. *Journal of Geophysical Research*, *79*(25), 3717. https://doi.org/10.1029/JA079i025p03717

Crooker, N. U., Larson, D. E., Kahler, S. W., Lamassa, S. M., & Spence, H. E. (2003). Suprathermal electron isotropy in high-beta solar wind and its role in heat flux dropouts. *Geophysical Research Letters*, *30*(12), 1619. https://doi.org/10.1029/2003GL017036

Fedorov, A. (2011). Transition and stability of high-speed boundary layers. *Annual Review of Fluid Mechanics*, *43*(1), 79–95. https://doi.org/10.1146/annurev-fluid-122109-160750

Foullon, C., Lavraud, B., Luhmann, J. G., Farrugia, C. J., Retinò, A., Simunac, K. D. C., … Sauvaud, J. A. (2011). Plasmoid releases in the heliospheric current sheet and associated coronal hole boundary layer evolution. *The Astrophysical Journal*, *737*, 16. https://doi.org/10.1088/0004-637X/737/1/16

Foullon, C., Lavraud, B., Wardle, N. C., Owen, C. J., Kucharek, H., Fazakerley, A. N., … Skoug, R. M. (2009). The apparent layered structure of the heliospheric current sheet: Multi-spacecraft Observations. *Solar Physics*, *259*(1–2), 389–416. https://doi.org/10.1007/s11207-009-9452-4

Galvin, A. B., Kistler, L. M., Popecki, M. A., Farrugia, C. J., Simunac, K. D. C., Ellis, L., … Steinfeld, D. (2008). The Plasma and Suprathermal Ion Composition (PLASTIC) investigation on the STEREO observatories. *Space Science Reviews*, *136*(1–4), 437–486. https://doi.org/10.1007/s11214-007-9296-x

Gonzalez, W. D., Joselyn, J. A., Kamide, Y., Kroehl, H. W., Rostoker, G., Tsurutani, B. T., & Vasyliunas, V. M. (1994). What is a geomagnetic storm? *Journal of Geophysical Research*, *99*(A4), 5771–5792. https://doi.org/10.1029/93JA02867

Gosling, J. T., Asbridge, J. R., Bame, S. J., & Feldman, W. C. (1978). Solar wind stream interfaces. *Journal of Geophysical Research*, *83*(A4), 1401–1412. https://doi.org/10.1029/JA083iA04p01401

Gosling, J. T., Skoug, R. M., McComas, D. J., & Smith, C. W. (2005). Direct evidence for magnetic reconnection in the solar wind near 1 AU. *Journal of Geophysical Research*, *110*, A01107. https://doi.org/10.1029/2004JA010809

Hoeksema, J. T. (1984). Structure and evolution of the large scale solar and heliospheric magnetic fields. PhD thesis, NASA, United States

Hoeksema, J. T., Wilcox, J. M., & Scherrer, P. H. (1983). The structure of the heliospheric current sheet—1978–1982. *Journal of Geophysical Research*, *88*, 9910–9918. https://doi.org/10.1029/JA088iA12p09910

Hu, Y. Q., & Jia, X. Z. (2001). Interplanetary shock interaction with the heliospheric current sheet and its associated structures. *Journal of Geophysical Research*, *106*(A12), 29,299–29,304. https://doi.org/10.1029/2001JA000112

Huang, J., Liu, Y. C.-M., Klecker, B., & Chen, Y. (2016). Coincidence of heliospheric current sheet and stream interface: Implications for the origin and evolution of the solar wind. *Journal of Geophysical Research: Space Physics*, *121*, 19–29. https://doi.org/10.1002/2015JA021729

Huang, J., Liu, Y. C.-M., Qi, Z., Klecker, B., Marghitu, O., Galvin, A. B., … Li, X. (2016). A multievent study of the coincidence of heliospheric current sheet and stream interface. *Journal of Geophysical Research: Space Physics*, *121*, 10,768–10,782. https://doi.org/10.1002/2016JA022842

Hundhausen, A. J. (1977). An interplanetary view of coronal holes. In J. B. Ziker (Ed.), *Coronal Holes and High Speed Wind Streams* (pp. 257–262). Boulder: Colorado Associated University Press.

Kaiser, M. L., Kucera, T. A., Davila, J. M., Cyr, O. C. S., Guhathakurta, M., & Christian, E. (2008). The STEREO mission: An introduction. In C. T. Russell (Ed.), *The STEREO Mission* (pp. 5–16). New York: Springer. https://doi.org/10.1007/978-0-387-09649-0_2

Khabarova, O. V. (2013). The interplanetary magnetic field: Radial and latitudinal dependences. *Astronomy Reports*, *57*(11), 844–859. https://doi.org/10.1134/S1063772913110024

Kilpua, E. K. J., Pomoell, J., Vourlidas, A., Vainio, R., Luhmann, J., Li, Y., … Simunac, K. (2009). STEREO observations of interplanetary coronal mass ejections and prominence deflection during solar minimum period. *Annales Geophysicae*, *27*(12), 4491–4503. https://doi.org/10.5194/angeo-27-4491-2009

Levy, E. H. (1976). The interplanetary magnetic field structure. *Nature*, *261*, June 3, 1976, 394–395. https://doi.org/10.1038/261394a0

Li, G. (2008). Identifying current-sheet-like structures in the solar wind. *The Astrophysical Journal Letters*, *672*(1), L65. https://doi.org/10.1086/525847

Liu, Y. C. M., Huang, J., Wang, C., Klecker, B., Galvin, A. B., Simunac, K. D. C., … Jian, L. (2014). A statistical analysis of heliospheric plasma sheets, heliospheric current sheets, and sector boundaries observed in situ by STEREO. *Journal of Geophysical Research: Space Physics*, *119*(11). https://doi.org/10.1002/2014JA019956

Lockwood, J. A., & Webber, W. R. (2005). Intensities of galactic cosmic rays of ~1.5 GV rigidity at Earth versus the heliospheric current sheet tilt. *Journal of Geophysical Research*, *110*, A04102. https://doi.org/10.1029/2004JA010880

Lowder, C., Qiu, J., Leamon, R., & Liu, Y. (2014). Measurements of EUV coronal holes and open magnetic flux. *The Astrophysical Journal*, *783*(2), 13. https://doi.org/10.1088/0004-637X/783/2/142

Luhmann, J. G., Curtis, D. W., Schroeder, P., McCauley, J., Lin, R. P., Larson, D. E., … Gosling, J. T. (2008). STEREO IMPACT investigation goals, measurements, and data products overview. *Space Science Reviews*, *136*(1–4), 117–184. https://doi.org/10.1007/s11214-007-9170-x

Malova, H. V., Popov, V. Y., Grigorenko, E. E., Dunko, A. V., & Petrukovich, A. A. (2016). Heliospheric current sheet and effects of its interaction with solar cosmic rays. *Plasma Physics Reports*, *42*(8), 749–760. https://doi.org/10.1134/S1063780X16080079

Maynard, N. C., Farrugia, C. J., Burke, W. J., Ober, D. M., Scudder, J. D., Mozer, F. S., … Siebert, K. D. (2011). Interactions of the heliospheric current and plasma sheets with the bow shock: Cluster and Polar observations in the magnetosheath. *Journal of Geophysical Research*, *116*, A01212. https://doi.org/10.1029/2010JA015872

McComas, D. J., Bame, S. J., Barker, P., Feldman, W. C., Phillips, J. L., Riley, P., & Griffee, J. W. (1998). Solar Wind Electron Proton Alpha Monitor (SWEPAM) for the Advanced Composition Explorer. *Space Science Reviews*, *86*, 563–612. https://doi.org/10.1023/A:1005040232597

McPherron, R. L., Terasawa, T., & Nishida, A. (1986). Solar wind triggering of substorm expansion onset, *IAGA*, Symposium on control of the solar-terrestrial interaction and magnetospheric substorm activity by the interplanetary medium, 5th, Prague, Czechoslovakia, Aug. 5–17, 1985. *Journal of Geomagnetism and Geoelectricity*, *38*(11), 1089–1108.

Nolte, J. T., & Roelof, E. C. (1973). Large-scale structure of the interplanetary medium. I: High coronal source longitude of the quiet-time solar wind. *Solar Physics*, *33*(1), 241–257. https://doi.org/10.1007/BF00152395

Opitz, A., Karrer, R., Wurz, P., Galvin, A. B., Bochsler, P., Blush, L. M., … Wimmer-Schweingruber, R. F. (2009). Temporal evolution of the solar wind bulk velocity at solar minimum by correlating the STEREO A and B PLASTIC measurements. *Solar Physics*, *256*, 365–377. https://doi.org/10.1007/s11207-008-9304-7

Owens, M. J., & Forsyth, R. J. (2013). The heliospheric magnetic field. *Living Reviews in Solar Physics*, *10*(1), 52. https://doi.org/10.12942/lrsp-2013-5

Owens, M. J., Crooker, N. U., & Lockwood, M. (2013). Solar origin of heliospheric magnetic field inversions: Evidence for coronal loop opening within pseudostreamers. *Journal of Geophysical Research: Space Physics*, *118*, 1868–1879. https://doi.org/10.1002/jgra.50259

Owens, M. J., Scott, C. J., Bennett, A. J., Thomas, S. R., Lockwood, M., Harrison, R. G., & Lam, M. M. (2015). Lightning as a space-weather hazard: UK thunderstorm activity modulated by the passage of the heliospheric current sheet. *Geophysical Research Letters*, *42*, 9624–9632. https://doi.org/10.1002/2015GL066802

Sauvaud, J. A., Larson, D., Aoustin, C., Curtis, D., Médale, J.-L., Fedorov, A., … Penou, E. (2008). The IMPACT Solar Wind Electron Analyzer (SWEA). In C. T. Russell (Ed.), *The STEREO Mission* (pp. 227–239). New York: Springer. https://doi.org/10.1007/978-0-387-09649-0_9

Schatten, K. H., Wilcox, J. M., & Ness, N. F. (1969). A model of interplanetary and coronal magnetic fields. *Solar Physics*, *6*, 442. https://doi.org/10.1007/BF00146478

Schrijver, C. J., & De Rosa, M. L. (2003). Photospheric and heliospheric magnetic fields. *Solar Physics*, *212*(1), 165–200. https://doi.org/10.1023/A:1022908504100

Schulz, M. (1973). Interplanetary sector structure and the helliomagnetic equator. *Astrophysics and Space Science*, *24*(2), 371–383. https://doi.org/10.1007/BF02637162

Simunac, K. D. C., Kistler, L. M., Galvin, A. B., Lee, M. A., Popecki, M. A., Farrugia, C., … Howard, R. A. (2009). In situ observations of solar wind stream interface evolution. *Solar Physics*, *259*(1–2), 323–344. https://doi.org/10.1007/s11207-009-9393-y

Smith, E. J. (2001). The heliospheric current sheet. *Journal of Geophysical Research*, *106*(A8), 15,819–15,832. https://doi.org/10.1029/2000JA000120

Smith, C. W., L'Heureux, J., Ness, N. F., Acuña, M. H., Burlaga, L. F., & Scheifele, J. (1998). The ACE magnetic fields experiment. *Space Science Reviews*, *86*, 613–632. https://doi.org/10.1023/A:1005092216668

Smith, E. J., Tsurutani, B. T., & Rosenberg, R. L. (1978). Observations of the interplanetary sector structure up to heliographic latitudes of 16°: Pioneer 11. *Journal of Geophysical Research*, *83*, 717–724. https://doi.org/10.1029/JA083iA02p00717

Stone, E. C., Frandsen, A. M., Mewaldt, R. A., Christian, E. R., Margolies, D., Ormes, J. F., & Snow, F. (1998). The Advanced Composition Explorer. *Space Science Reviews*, *86*(1/4), 1–22. https://doi.org/10.1023/A:1005082526237

Svalgaard, L., & Wilcox, J. M. (1975). Long-term evolution of solar sector structure. *Solar Physics*, *41*, 461–475. https://doi.org/10.1007/BF00154083

Thomas, S. R., Owens, M. J., Lockwood, M., Barnard, L., & Scott, C. J. (2015). Near-Earth cosmic ray decreases associated with remote coronal mass ejections. *The Astrophysical Journal*, *801*(1), 8. https://doi.org/10.1088/0004-637X/801/1/5

Thomas, B. T., & Smith, E. J. (1981). The structure and dynamics of the heliospheric current sheet. *Journal of Geophysical Research*, *86*(A13), 11,105–11,110. https://doi.org/10.1029/JA086iA13p11105

Tsurutani, B. T. & Gonzalez, W. D. (1997). The Interplanetary causes of magnetic storms: A review. *98*, 77–89. https://doi.org/10.1029/GM098p0077

Wang, Y.-M., & Sheeley, N. R. Jr. (1992). On potential field models of the solar corona. *Astrophysical Journal*, Part 1 (ISSN 0004-637X), *392*(1), 310–319. Research supported by U.S. Navy. https://doi.org/10.1086/171430

Zharkova, V. V., & Khabarova, O. V. (2012). Particle dynamics in the reconnecting heliospheric current sheet: Solar wind data versus three-dimensional particle-in-cell simulations. *The Astrophysical Journal*, *752*(1), 17. https://doi.org/10.1088/0004-637X/752/1/35